ACADEMIC PRESS

Available online at www.sciencedirect.com
SCIENCE DIRECT®

Journal of Catalysis 218 (2003) 438–446

JOURNAL OF CATALYSIS

www.elsevier.com/locate/jcat

Oxidative dehydrogenation of butane over nanocrystalline MgO, Al_2O_3, and VO_x/MgO catalysts in the presence of small amounts of iodine

Vladimir V. Chesnokov,[a] Alexander F. Bedilo,[b,*] David S. Heroux,[b] Ilya V. Mishakov,[a] and Kenneth J. Klabunde[b]

[a] *Boreskov Institute of Catalysis, Novosibirsk 630090, Russia*
[b] *Department of Chemistry, Kansas State University, Manhattan, KS 66506, USA*

Received 20 February 2003; accepted 24 February 2003

Abstract

High surface area nanocrystalline MgO, Al_2O_3, $MgO \cdot Al_2O_3$, commercial MgO, and a series of 10% V/MgO samples were used as catalysts in one-step selective oxidative dehydrogenation of butane to butadiene in the presence of oxygen and iodine. Molecular iodine shifts the equilibrium of the dehydrogenation reactions to the right and makes it possible to achieve high butane conversion with high selectivity to butadiene. When excess oxygen is present in the feed, iodine is successfully regenerated and can be recycled. Butadiene selectivity as high as 64% has been achieved in the presence of small amounts of iodine (0.25 vol%) over a vanadia–magnesia catalyst at 82% butane conversion. The best performance was observed over a catalyst containing the magnesium orthovanadate phase.

Keywords: Oxidative dehydrogenation; Butane; Iodine; Nanocrystalline oxide; VO_x/MgO

1. Introduction

Olefins and diene hydrocarbons (propene, butenes, isobutene, isoprene, butadiene, etc.) are widely used in various chemical processes for production of synthetic resins, plastics, gasoline components (methyl *tert*-butyl ether, methyl *tert*-amyl ether, alkylates), and other valuable products. For this reason, great interest in improving the existing methods for their production has remained steady for over 50 years. In particular, dehydrogenation of paraffins has been of interest in this regard.

The majority of methods used for dehydrogenation are catalytic. This fact accounts for a large number of studies devoted to development of new dehydrogenation catalysts and improvement of the existing ones [1–5]. Of special interest are catalysts for dehydrogenation of *n*-butane to butadiene.

There are several specific features of dehydrogenation reactions that limit choices of the reaction conditions, process engineering and type of catalysts. Dehydrogenation reactions of paraffins and olefins are very endothermic. The yields of desired products are usually limited by equilibrium conditions. Acceptable yields are typically achieved only above 520 °C for dehydrogenation of paraffins and above 570 °C for dehydrogenation of olefins. Therefore, dehydrogenation processes are usually carried out at very high temperatures (550–620 °C) where cracking of the hydrocarbons and carbon deposition on the catalysts become significant. In order to decrease the partial pressure of the starting hydrocarbons and increase the yield of the desired products, one-stage dehydrogenation of *n*-butane to butadiene is performed under vacuum over alumina–chromium catalysts [4,6].

Our analysis of the available approaches to butane dehydrogenation indicates that prospects for improvement of the conventional dehydrogenation method seem to be exhausted since butene and butadiene yields achieved are very close to the corresponding equilibrium values. In most processes employed, the butadiene content in the dehydrogenated C_4 stream from the reactor after separation of other by-products is limited to about 20%.

In the past few years numerous papers have appeared devoted to oxidative dehydrogenation of propane and butane [7–17]. Oxidative dehydrogenation of these hydrocarbons has a number of advantages in comparison with conventional dehydrogenation, such as high exothermicity that eliminates the need for heat supply to the reactor, removal of

* Corresponding author.
E-mail address: szura@ksu.edu (A.F. Bedilo).

0021-9517/03/$ – see front matter
doi:10.1016/S0021-9517(03)00085-X

the thermodynamic limitations on the yield of the desired products, decrease of the reactor temperature, and lower yields of side reactions (cracking and carbon deposition). Oxidative dehydrogenation of butane is usually performed over catalysts containing V [7–12] or Mo [15–17] on various supports. The best results so far have been obtained on a VO_x/MgO system [7]. However, the main problem of oxidative dehydrogenation—improvement of the selectivity to butadiene—remains unsolved.

In the present paper we demonstrate an increase in butadiene selectivity of this process by performing oxidative dehydrogenation in the presence of small amounts of iodine. The idea of "iodine dehydrogenation" was popular in the 1960s and 1970s. The key reagent in this case is molecular iodine that reacts with butane and butenes at about 500 °C to form butadiene and HI [18,19]. This idea was first researched by Shell Development at Emeryville, California, leading to a process concept known as Temescal, the name of an underground river which kept popping up in the most unexpected place. The main advantage of using iodine instead of other halogens is that the selectivity to cracking products and iodine-containing hydrocarbons is very low in this temperature range.

Further development of this approach involved introduction of an HI acceptor that could be easily regenerated by oxygen or air [20]. Many different oxides and hydroxides can be used as HI acceptors. The following reactions take place in the case of a group II metal oxide:

$$C_4H_{10} + I_2 + MO \rightarrow C_4H_8 + MI_2 + H_2O, \quad (1)$$

$$C_4H_8 + I_2 + MO \rightarrow C_4H_6 + MI_2 + H_2O, \quad (2)$$

$$2MI_2 + O_2 \rightarrow 2MO + 2I_2. \quad (3)$$

The use of an acceptor that reacts with HI easily and completely shifts the equilibrium of the dehydrogenation reactions to the right and makes it possible to achieve high butane conversion with high selectivity to butadiene. For example, it has been found that an increase of the oxygen concentration from 0 to 1.03 mol O_2/mol *n*-butane has a favorable effect on the butadiene yield [21]. Using Mn_3O_4/γ-Al_2O_3 acceptor and an I_2:C_4H_{10} molar ratio of 0.3 at 550 °C, the C_4H_6 yield based on *n*-C_4H_{10} fed was 20.0; 25.9 and 31.2 mol% for the O_2:C_4H_{10} molar ratios of 0; 0.26 and 0.97, respectively. At 0.45 I_2:C_4H_{10} ratio, the C_4H_6 yields increased to 34.7; 42.2 and 47.8%, correspondingly, under otherwise similar conditions.

Shell scientists have suggested a process based on the acceptor circulation in the reactor [22]. In this case, the acceptor was introduced into the bottom part of the reactor where it was regenerated with oxygen or air to yield molecular iodine. Then, it was transferred to the middle section of the reactor where it was mixed with butane. Butane dehydrogenation took place in the top part of the reactor with the formation of C_4H_6, HI, and some by-products. HI formed in the reaction was absorbed by the acceptor. Then, the gas–solid mixture was subjected to separation in cyclones, and the recovered acceptor was returned into the reactor. Despite the above advantages of iodine-mediated oxidative dehydrogenation, this method proved to be economically adverse due to significant losses of iodine and its high cost. Due to high iodine concentrations used, the yield of iodinated hydrocarbons could reach 0.10–0.15 kg per 1 kg of butadiene [23].

In this paper we suggest a different approach. In order to increase the efficiency of iodine-mediated oxidative dehydrogenation, we suggest combining the oxidative dehydrogenation, HI destructive adsorption by an acceptor, and I_2 regeneration in one place. This requires the catalyst acceptor to have oxidative properties and significant amounts of oxygen to be present in the feed.

Nanocrystalline metal oxides prepared by a modified aerogel procedure developed in our laboratory at KSU are known to have high surface areas, small crystallite sizes, unusual morphology, and enhanced adsorption properties in comparison with conventionally prepared materials [24–28]. These properties make them very good candidates for various applications as catalysts and catalyst supports. In the present paper we report our first results on the use of nanocrystalline MgO, Al_2O_3, and $MgO \cdot Al_2O_3$ as butane dehydrogenation cocatalysts and the use of nanocrystalline AP-MgO as a support for vanadium in the same reaction.

2. Experimental

2.1. Reagents and materials

Magnesium methoxide was prepared by dissolving Mg metal ribbon (Fisher) in methanol. Typically, 1 M solution was prepared by the reaction of 4.86 g (0.20 mol) Mg with 206 ml methanol under nitrogen flow at room temperature. After completion of the reaction, the reaction vessel was sealed and stored at room temperature for future use in the synthesis of aerogels.

For synthesis of AP-$Mg(OH)_2$, 43 ml of a 1 M $Mg(OCH_3)_2$ solution in methanol was mixed with 200 ml toluene in a glass beaker. The solution was homogenized by stirring with a magnetic stir bar for 10 min. Then, distilled deionized water used for hydrolysis was added dropwise to the solution. The water addition resulted in immediate formation of small amounts of white precipitate. After adding several drops of water, the mixture was stirred for several minutes until complete dissolution of the precipitate. The total amount of added water was 3.2 ml (0.2 mol). This corresponds to H_2O/Mg molar ratio of 5. The mixture was allowed to stir overnight prior to being subjected to supercritical drying.

For preparation of AP-$Al(OH)_3$, 4.4 g aluminum isopropoxide (Aldrich, 98%) was dissolved in a mixture containing 47 ml ethanol and 133 ml toluene. The mixture was stirred for about 1 h until complete disappearance of aluminum isopropoxide precipitate and formation of a homogeneous colloidal solution. Distilled deionized water (1.0 ml)

used for hydrolysis was added to 33 ml ethanol and stirred for 10 min. Then, this solution was quickly added to the aluminum isopropoxide solution. The resulting gel was stirred overnight before supercritical drying.

For preparation of a mixed aluminum–magnesium hydroxide aerogel, 2.2 g aluminum isopropoxide (Aldrich, 98%) was dissolved in a mixture containing 50 ml methanol and 135 ml toluene similar to the above procedure for synthesis of AP-Al(OH)$_3$. Then, 10.7 ml of 1 M Mg(OCH$_3$)$_2$ solution in methanol was added to the solution and homogenized for 10 min. Hydrolysis was performed by fast addition of 1.0 ml water dissolved in 20 ml methanol followed by overnight stirring.

The aerogels were prepared by high temperature supercritical drying of the gels in a standard 1-liter autoclave (Parr). The autoclave with the gel was first flushed with nitrogen for 10 min. Then it was filled with nitrogen at an initial pressure of about 700 kPa and sealed. The autoclave temperature was slowly increased up to 265 °C at a rate of 1 K per minute and maintained at that temperature for 10 min. After completion of the procedure, the pressure was quickly released by venting of solvent vapor. The sample was again flushed with nitrogen for 10 min and allowed to cool down in nitrogen. The final step for preparation of the oxides was overnight evacuation of the corresponding hydroxides at 500 °C.

CP-MgO was obtained by decomposition of Mg(OH)$_2$ prepared by overnight hydration of commercial MgO (Aldrich) in refluxing water followed by evacuation at 500 °C. Performance of high surface area MgO materials was compared to that of a commercial low surface area sample CM-MgO (Aldrich, 99.99%, S.A. 18 m^2/g).

Since the preliminary experiments have shown that AP-MgO had the best catalytic/acceptor properties, it was used as a support for vanadia catalysts. The catalysts used contained ∼ 10 wt% V and were prepared by three different methods.

Vanadium precursors: vanadyl acetylacetonate (Aldrich, 99%), vanadium oxytriisopropoxide (Aldrich), and ammonium vanadate (Acros) were used without further processing. Solvents: reagent grade THF and toluene (both Fisher) were dried over molecular sieves.

VO_x/MgO sample with V(acac)$_3$ used as a precursor was prepared as follows. Four hundred milliliters of dried THF was added to a 500-ml Erlenmeyer flask in an argon atmosphere. The precursor was then weighed and added to the THF. The THF solution of vanadium acetylacetonate was stirred for at least 1 h until the entire precursor dissolved. MgO was then added with stirring to the V(acac)$_3$ solution, and stirring was continued under argon for at least 12 h. The VO_x/MgO catalyst was then filtered in a Buchner funnel attached to a water aspirator to remove the solvent and excess V(acac)$_3$. The final preparation step for all VO_x/MgO samples was calcination at 600 °C in air for 2 h. This sample will be denoted as VO_x/MgO-1.

The sample using the VO(OPr^i)$_3$ precursor (VO_x/MgO-2) was prepared as follows. The support was placed in a Schlenk flask in an atmosphere of argon. Dried toluene was then added to the Schlenk flask. The support was mixed for 1 h to fully disperse the MgO particles. The VO(OPr^i)$_3$ was stored in a dry box. A swage-lock syringe was introduced to the dry box and the desired amount of precursor was syringed. The syringe was then closed and removed from the dry box. While a current of argon was flowing through the Schlenk flask, the precursor was syringed into the stirring MgO toluene suspension. The sample was stirred overnight. Then, the toluene was removed at reduced pressure using a vacuum line at room temperature followed by calcination at 600 °C.

VO_x/MgO sample prepared from the ammonium vanadate precursor was synthesized following a method described by Chaar et al. [9]. AP-MgO powder was impregnated with a solution containing 1 wt% of ammonium vanadate and 0.5 wt% of ammonium hydroxide. The resulting suspension was evaporated with stirring until a paste was obtained. This paste was dried at 120 °C and then calcined at 600 °C. The catalyst prepared by this method will be designated hereafter as VO_x/MgO-3.

2.2. Catalytic experiments

The performance of different catalysts in iodine-mediated oxidative dehydrogenation was studied in a 10 cm^3 quartz flow reactor. The reactor was placed inside an electrical furnace. The reaction was carried out in the temperature range of 500–580 °C. The catalyst loadings were varied between 0.05 and 0.8 g. The feed flow rate was 10 L/h. The catalysts were diluted with quartz powder to prevent removal of the oxide particles by the gas flow. The composition of the feed (vol%) was 92.5% He:2.5% C_4H_{10}:5% O_2.

The iodine concentration in the feed was varied between 0 and 0.25 vol%. The feed was saturated with iodine in a bubbler maintained at a certain temperature (room temperature or 50 °C). The gas line between the bubbler and the reactor was heated to prevent iodine condensation on the walls. The concentration of iodine in the feed was estimated gravimetrically from the loss of iodine in the bubbler after a certain time on stream. This procedure was performed several times at each temperature and the average value was taken. The results obtained are in a good agreement with those calculated from the iodine vapor pressure.

The experiments were performed in the following order. First, oxidative dehydrogenation of butane was studied without any iodine for about 1 h. During the next hour the feed was passed through the bubbler with iodine maintained at room temperature. The iodine concentration in the feed was measured to be about 0.1 vol%. At the final stage, the bubbler temperature was increased to 50 °C to give 0.25 vol% iodine in the feed.

The exit gases from reactor were analyzed by gas chromatography using a GOW MAC 580 chromatograph equip-

ped with a TCD detector, Chromosorb CP-AW and Molecular Sieve columns. The data were collected and analyzed using DT2804 data acquisition board by Justice Innovation and Chrom Perfect software package.

2.3. Characterization of samples

Textural characterization of the samples was performed on a NOVA 1200 gas sorption analyzer (Quantachrome Corp.). Prior to the analysis the samples were outgassed at 250 °C for 1 h. Seven-point BET surface areas, total pore volumes, and average pore diameters were calculated from nitrogen adsorption isotherms.

X-ray powder diffraction experiments were conducted on a Scintag-XDS-2000 spectrometer with Cu-K_α radiation. Scans were made in the 2Θ range 20–80° with a scanning rate of 1° per minute. Crystallite sizes were determined from X-ray line broadening using the Scherrer equation with correction for the instrument broadening. The error in the evaluation of the average crystallite sizes by XRD is about 0.1 nm for the samples with small crystallite sizes and about 0.2 nm for the sample with 20 nm crystals.

A scanning electron microscope (SEM, Hitachi Science System, S-3500N) was used for determination of the elemental composition of vanadia-doped samples. The samples were deposited onto a sticking pad. Energy dispersive analysis (EDXA) with 20 keV electron acceleration voltage provided determination of the elemental composition up to 10–15 monolayers in depth. The resolution of the SEM instrument was not sufficient to distinguish individual nanoparticles; therefore, it was not possible to evaluate the particle size from SEM images.

Raman spectra were collected using a Nicolet Nexus 670 FTIR spectrometer with an FT-Raman attachment. The laser energy was 0.4 W at a wavelength of 1064 nm. The spectra were recorded using 1024 scans at 4 cm^{-1} resolution.

UV–visible spectra were recorded using a Varian Cary 500 spectrophotometer with a diffuse reflectance attachment. The spectra were collected in the range of 200–2500 nm with 600 nm/min scan rate. Polytetrafluoroethylene (Aldrich) was used as a reference material.

3. Results and discussion

3.1. Characterization of materials by physical methods

AP-MgO has been extensively characterized by a variety of physical methods in previous publications [24–26]. Details on the development of synthetic procedures and characterization of several AP-Al_2O_3 and AP-MgO–Al_2O_3 samples have been also reported recently and will not be discussed here [28]. Textural characteristics of all samples reported in this paper are presented in Table 1.

As will be discussed below, catalytic properties of vanadia–magnesia samples proved to depend significantly on the preparation technique, which affects the state of vanadium in the final catalyst. A scanning electron microscope study has shown that initial aerogel MgO crystals are subjected to significant changes after vanadium deposition. The most significant changes were observed for VO_x/MgO-1. This is in good agreement with the most significant decrease in the surface area of the sample. The following magnesium/vanadium atomic ratios have been obtained for different samples with the formal 10 mol% vanadium loading: Mg/V = 3 for VO_x/MgO-3, Mg/V = 4.8 for VO_x/MgO-1, and Mg/V = 10 for VO_x/MgO-2. The lowest vanadium concentration found on the surface of the catalyst prepared from vanadium oxytriisopropoxide is, most likely, due to its higher surface area. It appears to indicate a more homogeneous distribution of vanadium on the surface of MgO nanocrystals. Surface ratios Mg/V = 3 and Mg/V = 4.8 are much closer to the ratio Mg/V = 1.5 corresponding to stoichiometric magnesium orthovanadate—$Mg_3(VO_4)_2$.

Table 1
Textural properties of materials studied

Sample	Surface area (m^2/g)	Pore volume (cm^3/g)	Average pore diameter (Å)
CM-MgO	18	0.06	132
CP-MgO	275	0.47	69
AP-MgO	460	0.54	47
AP-Al_2O_3	815	1.70	83
AP-MgO–Al_2O_3	820	1.54	75
VO_x/MgO-1	100	0.54	215
VO_x/MgO-2	230	0.76	131
VO_x/MgO-3	140	0.41	115

Fig. 1 presents XRD profiles of 10% V/MgO catalysts and AP-MgO. For all the samples, the two main peaks observed at 43 and 62° correspond to the MgO phase. The spectra indicate that the particle size increases in the follow-

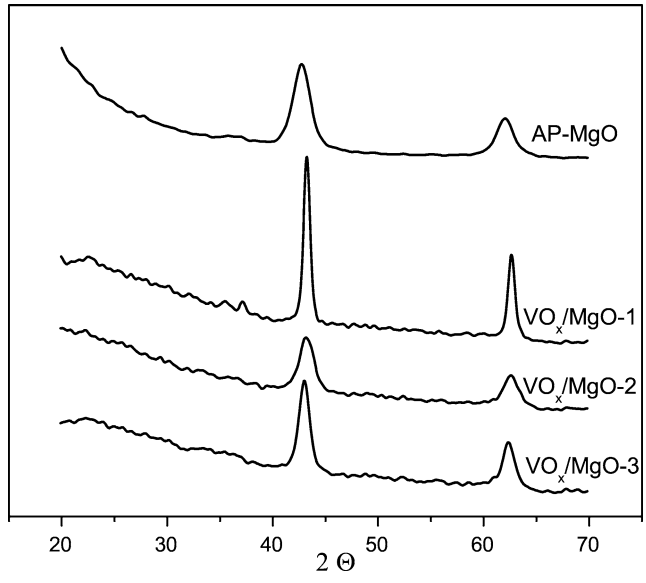

Fig. 1. XRD profiles of AP-MgO and VO_x/AP-MgO samples.

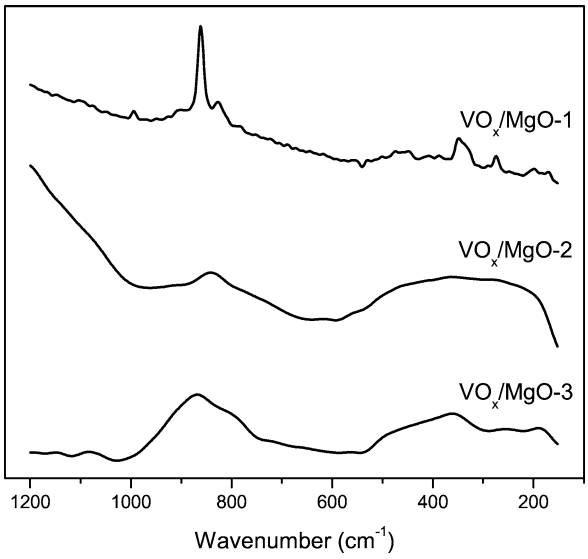

Fig. 2. Raman spectra of VO_x/AP-MgO samples.

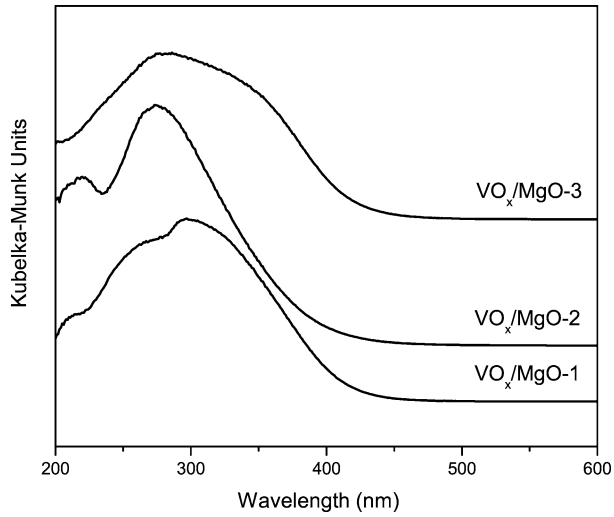

Fig. 3. Diffuse reflectance UV–vis spectra of VO_x/AP-MgO samples.

ing order: VO_x/MgO-2 < VO_x/MgO-3 < VO_x/MgO-1. The estimated average crystallite sizes are 6.0, 8.5, and 20.6 nm, respectively. The fact that all of these average sizes are larger than that of the initial AP-MgO, which is about 4.5 nm, indicates significant sintering of the MgO particles during the vanadium deposition procedure. This sintering is apparently most intense when vanadium is deposited from V(acac)$_3$ in THF. In addition, this catalyst exhibits two additional small peaks at 35.5 and 37°, indicating the presence of magnesium orthovanadate $Mg_3(VO_4)_2$. Minimum sintering is observed for sample VO_x/MgO-2, its average crystallite size being close of that of the pure MgO support heated at 600 °C in air.

Raman spectra of V/AP-MgO samples are presented in Fig. 2. AP-MgO does not exhibit any lines in the Raman spectrum. The spectrum of VO_x/MgO-1 has clearly defined lines at 862 (most intense), 827, 350, and 275 cm^{-1} that can be attributed to the $Mg_3(VO_4)_2$ phase [29,30].

In the spectrum of VO_x/MgO-3 there are two wide peaks at 360 and 870 cm^{-1}. Most likely, they are also related to the $Mg_3(VO_4)_2$ phase with smaller particle size than in the case of VO_x/MgO-1. The peak positions are close to those observed for the above sample, while due to larger linewidth only the most intense peaks can be distinguished. Small nanoparticles in crystalline materials are known to have wider lines in the Raman spectra, although exact size determination from their width is usually impossible.

The Raman spectrum of VO_x/MgO-2 has a wide halo in the area of 330–380 cm^{-1} and a peak at 830 cm^{-1} with a shoulder at about 860 cm^{-1}. The peak at 830 cm^{-1} can be assigned to V–O–M (M = Mg or V) vibration of tetrahedrally coordinated VO_4 species [8,31,32]. The halo and the shoulder at 860 cm^{-1} seem to indicate the presence of the $Mg_3(VO_4)_2$ phase with very small particle size or low crystallinity.

Thus, the technique used for preparation of V/AP-MgO catalysts has a very significant effect on the state of vanadium. The first two samples seem to have the same $Mg_3(VO)_4$ crystalline phase with different particle size. Meanwhile, in VO_x/MgO-2 vanadium atoms are mainly present at the surface of MgO as isolated VO_4 species.

Diffuse reflectance UV–vis spectra of the samples are presented in Fig. 3. Although the spectra look slightly different, all of them can be assigned to CT transitions of tetrahedrally coordinated V^{5+} ions [12,33]. This is in agreement with both $Mg_3(VO_4)_2$ phase and isolated VO_4 species in tetrahedral coordination. Meanwhile, the formation of $Mg_2V_2O_7$ or V_2O_5 in significant amounts can be reliably excluded.

3.2. Butane dehydrogenation over nanocrystalline oxides without vanadium

Prior to investigating the catalytic properties of oxides and vanadium–magnesia samples, we have performed analysis of the reactions taking place in a reactor filled with low surface area broken quartz with different amounts of iodine (Table 2). One can see that no noncatalytic reaction takes place (in the absence of heterogeneous catalyst and/or iodine). Addition of 0.1 vol% iodine results in the appearance of some cracking and dehydrogenation reactions with only 5% conversion, with cracking being a predominant process. An increase of the iodine concentration in the

Table 2
Effect of the iodine concentration in the feed on the butane conversion and selectivity of oxidative dehydrogenation over broken quartz (C_4H_{10} = 2.5%, O_2 = 5%, T = 550 °C, P_{cat} = 0.4 g)

I_2 concentration	Conversion	Selectivity (%)			
(%)	(%)	C_4H_6	C_4H_8	C_1–C_3	CO + CO_2
0	0	0	0	0	0
0.1	5	20	30	50	0
0.25	20	54	16	30	0

feed to 0.25% results in higher butane conversion and a significant change of the process selectivity. In this case the selectivity to dehydrogenation products ($C_4H_8 + C_4H_6$) is as high as 70%.

It is important to note that the amount of butadiene formed exceeds the stoichiometric amount corresponding to reaction (4):

$$C_4H_{10} + 2I_2 \rightarrow C_4H_6 + 4HI. \quad (4)$$

Since the iodine content in the feed is only 10% of that of butane, the amount of butadiene formed according to reaction (4) should not exceed 5%. Meanwhile, the actual butadiene yield is 10.8%. This fact indicates that iodine acts, at least partially, as a homogeneous catalyst. Apparently, oxygen reacts with HI faster than it does with hydrocarbons, regenerating some iodine according to reaction (5):

$$4HI + O_2 \rightarrow H_2O + 2I_2. \quad (5)$$

This internal iodine regeneration is the reason for higher butadiene yield. Still, without a cocatalyst the butane conversion is very low, and much of the iodine leaves the reactor in the form of HI and has to be somehow regenerated later.

As a basic material, MgO is a good candidate for an HI acceptor that can take it out of the feed and yield I_2 upon reaction with oxygen. We have studied the catalytic properties of three MgO samples with very different surface areas that were prepared by different techniques. Fig. 4 presents the dependence of butane conversion on the MgO loading. One can see that the conversion grows with a loading increase for all the samples, although this dependence is far from linear. We believe that the lack of linearity reflects the approach of the dehydrogenation reaction to equilibrium. It is also evident that the activity of high surface area nanocrystalline AP-MgO is much higher than that of CM-MgO.

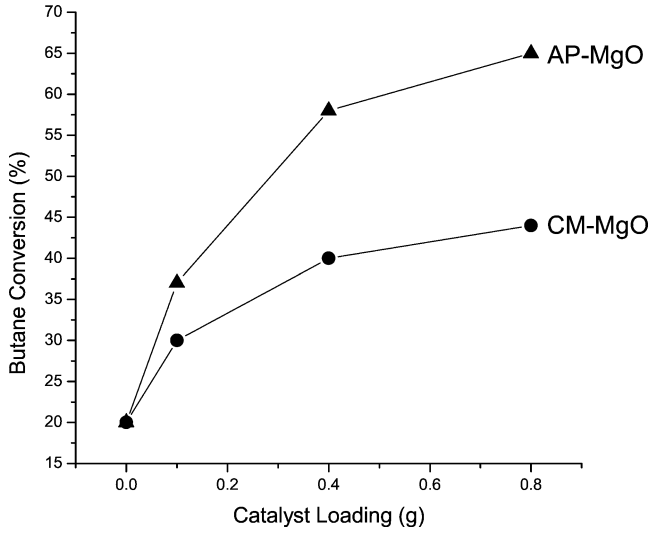

Fig. 4. Effect of catalyst loading on butane conversion at 550 °C over different MgO samples. Feed composition (vol%): 92.25% He, 2.5% C_4H_{10}, 5% O_2, and 0.25% I_2.

Table 3
Effect of the iodine concentration in the feed on the butane conversion and selectivity of oxidative dehydrogenation over different MgO samples, AP-$MgO \cdot Al_2O_3$ and AP-Al_2O_3 (C_4H_{10} = 2.5%, O_2 = 5%, T = 550 °C, P_{cat} = 0.4 g)

Catalyst	I_2 concentration (%)	Conversion (%)	Selectivity (%)			
			C_4H_6	C_4H_8	C_1–C_3	CO + CO_2
CM-MgO	0	0	0	0	0	0
	0.1	16	18	16	56	10
	0.25	40	60	5	30	5
CP-MgO	0	12	0	0	85	15
	0.1	23	24	4	54	18
	0.25	46	55	4	36	5
AP-MgO	0	28	0	0	80	20
	0.1	40	17	8	60	15
	0.25	58	64	5	22	9
AP-$MgO \cdot Al_2O_3$	0	26	0	0	85	15
	0.1	35	20	4	60	16
	0.25	60	45	3	34	18
AP-Al_2O_3	0	17	3	9	70	18
	0.1	24	15	10	60	15
	0.25	35	28	0	45	27

The results illustrating the effect of iodine on the performance of the metal oxide samples in oxidative dehydrogenation of butane are summarized in Table 3. The relative activity of the MgO samples follows the order of their surface areas: AP-MgO > CP-MgO > CM-MgO. This dependence holds both in the presence of iodine and in its absence. The activity of CM-MgO is very low. As in the case of quartz, no reactions take place over CM-MgO without iodine. Butadiene selectivity does not depend on the type of MgO. Meanwhile, it grows considerably with an increase of the iodine concentration. The only difference between the MgO samples is in their activity. Higher butane conversion over AP-MgO results in higher butadiene yield (product of butane conversion and butadiene selectivity).

When other high surface area nanocrystalline oxides (AP-$MgO \cdot Al_2O_3$, AP-Al_2O_3) were used, the activity and selectivity of oxidative dehydrogenation also grew with an increase of the iodine concentration, although this effect was significantly less pronounced. The lowest selectivity was observed over the alumina sample, indicating that Al_2O_3 is not a good catalyst for this reaction. The performance of mixed $MgO \cdot Al_2O_3$ was intermediate between AP-MgO and AP-Al_2O_3.

Fig. 5 illustrates the dependence of the butadiene yield on the iodine concentration for all oxides studied. Nanocrystalline AP-MgO is clearly the best catalyst among them.

The following conclusions can be made on the role of MgO in iodine-mediated oxidative dehydrogenation of butane. It is well known that for activation of a butane molecule one has to detach a hydrogen atom. Such butane activation may be initiated both by iodine atoms, as in the case of reactor filled with quartz, and by basic sites on the MgO surface. It is well known that MgO is capable of generating butyl radicals from butane.

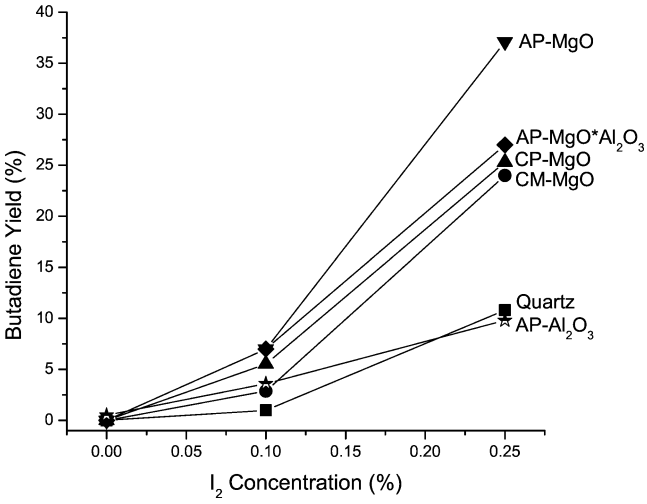

Fig. 5. Effect of iodine concentration in the feed on butadiene yield over different catalysts at 550 °C and catalyst loading 0.4 g.

The butyl radicals can undergo further transformation leading either to cracking or to dehydrogenation products. The first process predominates when there is no iodine or its concentration does not exceed 0.1%. When the iodine concentration is higher, there is a high probability for butyl radicals to react with iodine to form iodobutane. The latter has been shown to undergo easy dehydroiodination over AP-MgO at temperatures above 300 °C to form butene and HI.

Iodine can be regenerated from HI by oxygen according to reaction (5). Generally speaking, this reaction does not require a catalyst, as shown above. However, a catalyst selective for HI oxidation would accelerate the iodine regeneration considerably. This would allow iodine to get involved into more catalytic cycles and significantly decrease its loss in the form of HI. If iodine did not act as a dehydrogenation catalyst, the amount of butadiene formed in reaction (4) at the iodine concentration in the feed, 10% of that of butane, would be one-half of this value, i.e., 5 mol%. The actual butadiene yield of 40% means that an average iodine molecule undergoes about 8 turnovers in the reactor. Thus, MgO seems to have a double effect during the iodine-mediated butane dehydrogenation—it accelerates the formation of butyl radicals and contributes to the iodine regeneration from HI.

With iodine present in the feed, butenes are subjected to further dehydrogenation to butadiene. We do not know for sure the exact mechanism of this reaction. The fact is that in the presence of 0.25% iodine, butenes are not accumulated, so that their concentration after the reactor is an order of magnitude lower than that of butadiene.

A comparison of the catalytic properties of MgO and Al_2O_3 indicates that alumina has more pronounced oxidative catalytic properties, so that both HI and hydrocarbons are oxidized. This makes the selectivity of AP-Al_2O_3 in iodine-mediated dehydrogenation of butane much lower than that of any MgO sample. For this reason, we did not study VO_x/Al_2O_3, limiting ourselves to the investigation of the VO_x/MgO system.

It is important to note that we did not detect any measurable amounts or iodinated organic compounds or HI after the reactor under the reaction conditions studied with nanocrystalline oxides used as catalysts. It means that molecular iodine is successfully regenerated over the catalysts in the presence of oxygen. Then, it can be easily separated from the organic fraction and recycled. So far, we have not made any attempts to recycle iodine and estimate its loss in the process, but the apparent lack of by-products containing iodine suggests that it can be made very low.

Excess of oxygen had to be maintained in the reactor in order to provide full iodine regeneration and prevent coke deposition on the catalysts. In fact, the oxygen concentration in the feed was adjusted to the value necessary for effective I_2 regeneration, which was then used in all experiments. At lower oxygen concentrations in the feed significant amounts of HI and iodinated hydrocarbons as well as some coke formation were observed. Typical oxygen consumption was 40–45% (2–2.5 L/h) for the best samples with 0.25% iodine concentration. Good material balance with respect to oxygen and carbon was observed for all reactions reported in the paper. So, the formation of undetected organic products in considerable amounts can be reliably excluded.

3.3. Butane dehydrogenation over VO_x/AP-MgO

The performance of different oxide samples described above is compared with that of VO_x/MgO-1 in Fig. 6. The vanadia–magnesia catalyst has much higher activity than any of the above oxides. Its activity is about 8 times higher than that of AP-MgO, while the butadiene selectivity is about the same at high iodine concentration (Fig. 7). The presence of vanadium is required for the appearance of a noticeable dehydrogenation activity without iodine.

A comparison of the catalytic activities of three 10% V/AP-MgO samples prepared from different vanadium precursors shows a difference in their properties (Table 4). The

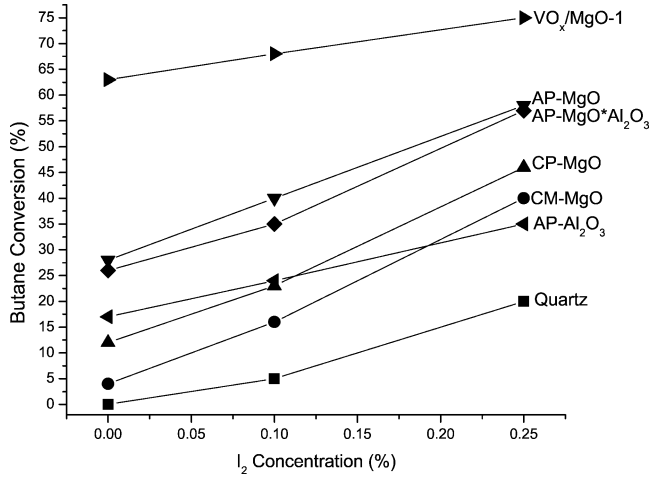

Fig. 6. Activity of different catalysts in butane dehydrogenation vs iodine concentration in the feed at 550 °C and catalyst loading 0.4 g.

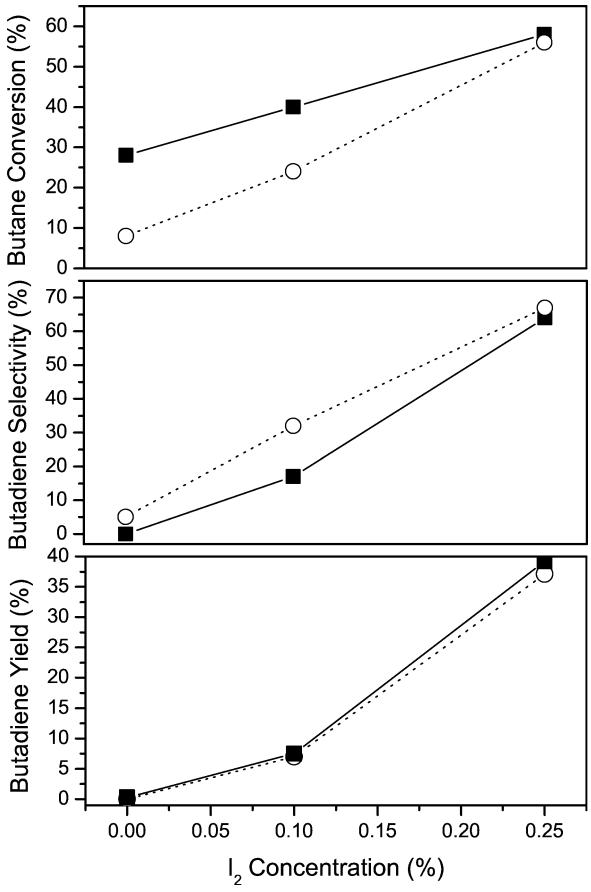

Fig. 7. Effect of iodine concentration in the feed on butane conversion, butadiene selectivity, and butadiene yield at 550 °C over VO_x/MgO-1 ((■) catalyst loading 0.05 g) and AP-MgO ((○) catalyst loading 0.4 g).

highest butadiene selectivity was observed for 10% V/AP-MgO prepared from V(acac)$_3$ (VO_x/MgO-1) where vanadium is present in the form of well-crystallized $Mg_3(VO_4)_2$. The sample prepared from $VO(OPr^i)_3$ (VO_x/MgO-2) has the lowest selectivity of the three. This sample contains a significant amount of isolated VO_4 species in tetrahedral coordination that are active in deep oxidation of butane, most likely due to weaker bonding between oxygen and vanadium than in $Mg_3(VO_4)_2$. Isolated VO_4 ions are known to be reduced at lower temperatures than vanadium in nanocrystalline $Mg_3(VO_4)_2$ [7,8].

Table 4
Effect of the iodine concentration in the feed on the butane conversion and selectivity of oxidative dehydrogenation over VO_x/AP-MgO catalysts ($C_4H_{10} = 2.5\%$, $O_2 = 5\%$, $T = 550$ °C, $P_{cat} = 0.05$ g)

Catalyst	I_2 concentration (%)	Conversion (%)	Selectivity (%)				
			C_4H_6	C_4H_8	C_2	[a]	CO + CO_2
VO_x/MgO-1	0	8	5	20	7	48	20
	0.1	24	32	10	5	41	12
	0.25	56	67	3	4	20	6
VO_x/MgO-2	0	36	15	10	4	31	40
	0.1	50	28	7	5	35	25
	0.25	60	37	3	4	38	18
VO_x/MgO-3	0	30	13	15	5	47	20
	0.1	45	26	12	5	43	14
	0.25	55	45	3	4	36	12

[a] Partial oxidation according to reaction (6).

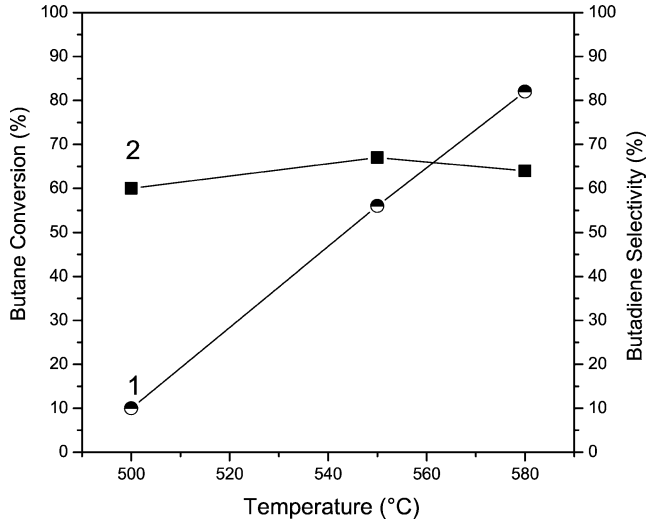

Fig. 8. Effect of reaction temperature on butane conversion (1) and butadiene selectivity (2) over VO_x/MgO-1 (catalyst loading 0.05 g, iodine concentration 0.25%).

An unusual distribution of cracking products is another feature typical for the iodine-mediated oxidative dehydrogenation over V/AP-MgO catalysts. In most cases, the propane concentration in the reaction products is abnormally high, while no methane is observed. It appears that propane is formed by partial oxidation of butane according to reaction (6):

$$C_4H_{10} + \tfrac{3}{2}O_2 = C_3H_8 + CO_2 + H_2O. \quad (6)$$

The butadiene selectivity of VO_x/MgO-1 does not change much when the reaction temperature is increased from 500 to 580 °C. Meanwhile, the butane conversion grows from 12% at 500 °C to 86% at 580 °C (Fig. 8).

The different mechanisms proposed for oxidative dehydrogenation of butane over VO_x/MgO catalysts [10,34–36] without iodine involve the generation of abundant surface OH groups as V–OH. It seems to be generally accepted that the initial step of butane reaction with an oxidized VO_x/MgO catalyst is the abstraction of an H atom to give an adsorbed butyl group. In the presence of iodine the butyl group can react either with iodine to give iodobutane or with oxygen to give carboxylate. Infrared spectroscopy studies of the surface suggests that this adsorption could take place as a carboxylate, similar to the configuration proposed by Busca [35]. Iodobutane is converted on the catalyst surface to butene and HI. Subsequent reaction between HI and surface oxygen atoms results in the formation of water and molecular iodine.

Thus, the effect of VO_x/MgO catalysts on iodine-mediated butane dehydrogenation is similar to that of magnesium oxide. The addition of this catalyst accelerates butane acti-

vation and iodine regeneration from HI. If the catalyst contains isolated vanadium ions in the tetrahedral coordination, its selectivity to butadiene is fairly low, most likely due to acceleration of the carbon chain partial oxidation according to reaction (6) or deep oxidation to form CO and CO_2. VO_x/MgO catalysts with a surface layer of $Mg_3(VO_4)_2$ combine high butadiene selectivity with relatively high activity.

4. Conclusions

The results obtained in this study for iodine-mediated oxidative dehydrogenation of butane over vanadia–magnesia catalysts are very promising for future practical application of this approach. Very high selectivity to butadiene can be achieved in the presence of iodine. When excess oxygen is present in the feed, molecular iodine is successfully regenerated and can be recycled.

Results slightly superior to ours (butadiene yield as high as 60% at butane conversion 76%) have been reported only for iodine-mediated dehydrogenation in a reactor with a circulating acceptor [22]. However, this process has a number of important drawbacks. Most important, production of 1 mol of butadiene (FW 54) requires 2 mol of iodine (FW 254). Hence per ton of butadiene produced there must be at least 9.4 tons of iodine present in the gases passing through the reactor. This results in very significant iodine losses due to the formation of iodoorganic compounds in considerable amounts.

Results comparable to ours have been reported for a fixed-bed Mn_3O_4/Al_2O_3 catalysts at a significantly higher iodine concentration ($I_2/C_4H_{10} = 0.3$) than the one used by us ($I_2/C_4H_{10} = 0.1$) [21]. Our results clearly indicate that the butadiene yield grows substantially with an increase of the iodine concentration in the range studied by us. It is very likely that in our experiments we have not reached the optimum iodine concentration. This will be explored in the future along with a more thorough study of iodine regeneration.

Besides butadiene, this method can be potentially applied for synthesis of many other olefins, e.g., propene, isobutene, or isoprene.

Acknowledgments

We gratefully acknowledge CRDF, NSF, and the Army Research Office (ARO) for financial support.

References

[1] I.Ya. Tyuryaev, Theoretical Bases for Synthesis of Butadiene and Isoprene by Dehydrogenation Methods, Naukova Dumka, Kiev, 1973 (in Russian).
[2] G.P. Kotelnikov, L.V. Strunnikova, V.A. Patanov, I.P. Arapova, Catalysts for Dehydrogenation of Lower Paraffin, Olefin and Alkyl Aromatic Hydrocarbons, TsNIITEneftekhim, Moscow, 1978 (in Russian).
[3] N.R. Bursian, S.B. Kogan, Uspekhi Khimii 58 (1989) 451.
[4] R.A. Buyanov, N.A. Pakhomov, Kinet. Catal. 42 (2001) 64.
[5] M.M. Bhasin, J.H. McCain, B.V. Vora, T. Imai, P.R. Pujado, Appl. Catal. A 221 (2001) 397.
[6] B.M. Weckhuysen, R.A. Schoonheydt, Catal. Today 51 (1999) 223.
[7] C. Tellez, M. Abon, J.A. Dalmon, C. Mirodatos, J. Santamaria, J. Catal. 195 (2000) 113.
[8] C. Pak, A.T. Bell, T.D. Tilley, J. Catal. 206 (2002) 49.
[9] M.A. Chaar, D. Patel, H.H. Kung, J. Catal. 109 (1987) 483.
[10] H.H. Kung, Adv. Catal. 40 (1994) 1.
[11] H.H. Kung, M.C. Kung, Appl. Catal. A 157 (1997) 105.
[12] T. Blasco, J.M. López Nieto, A. Dejoz, M.I. Vazquez, J. Catal. 157 (1995) 271.
[13] L.M. Madeira, M.F. Portela, Catal. Rev. 44 (2002) 247.
[14] P. Rybarczyk, H. Berndt, J. Radnik, M.-M. Pohl, O. Buyevaskaya, M. Baerns, A. Bruckner, J. Catal. 202 (2001) 45.
[15] R.M. Martin-Aranda, M.F. Portela, L.M. Madeira, F. Freire, M. Oliveira, Appl. Catal. A 127 (1995) 201.
[16] G.E. Vrieland, C.B. Murchison, Appl. Catal. A 134 (1996) 101.
[17] G.E. Vrieland, B. Khazai, C.B. Murchison, Appl. Catal. A 134 (1996) 123.
[18] Shell Development Co., Canadian patent 576172, 1955.
[19] Shell Development Co., US patent 2890253, 1956.
[20] Shell International Research Maatschappij N.V., British patent 895500, 1959.
[21] G.A. Stepanov, V.A. Kolobikhin, M.I. Myasoedov, R.V. Chugunnikova, Neftekhimiya 5 (1965) 815.
[22] R.W. King, Hydrocarbon Process. 45 (11) (1966) 189.
[23] R. King, Proc. Engin. March (1977) 85.
[24] S. Utamapanya, K.J. Klabunde, J.R. Schlup, Chem. Mater. 3 (1991) 175.
[25] K.J. Klabunde, J.V. Stark, O.B. Koper, C. Mohs, D.G. Park, S. Decker, Y. Jiang, J. Lagadic, D. Zhang, J. Phys. Chem. 100 (1996) 12142.
[26] R. Richards, W. Li, S. Decker, C. Davidson, O. Koper, V. Zaikovskii, A. Volodin, T. Rieker, K.J. Klabunde, J. Am. Chem. Soc. 122 (2000) 4921.
[27] O.B. Koper, J. Lagadic, A.M. Volodin, K.J. Klabunde, Chem. Mater. 9 (1997) 2468.
[28] C.L. Carnes, P.N. Kapoor, K.J. Klabunde, J. Bonevich, Chem. Mater. 14 (2002) 2922.
[29] G. Ramis, G. Busca, V. Lorenzelli, J. Chem. Soc., Faraday Trans. 90 (1994) 1293.
[30] G. Busca, G. Ricchiardi, D.S.W. Sam, J.C. Volta, J. Chem. Soc., Faraday Trans. 90 (1994) 1161.
[31] G. Deo, I.E. Wachs, J. Phys. Chem. 95 (1991) 5889.
[32] M.K. Yurdakoc, R. Haffner, D. Honicke, Mater. Chem. Phys. 44 (1996) 273.
[33] G. Centi, S. Perathoner, F. Trifiró, A. Aboukais, C.F. Aissi, M. Guelton, J. Phys. Chem. 96 (1992) 2617.
[34] T. Blasco, J.M. López Nieto, Appl. Catal. A 157 (1997) 17.
[35] G. Busca, Catal. Today 27 (1996) 457.
[36] J.M. López Nieto, P. Concepción, A. Dejoz, H. Knozinger, F. Melo, I. Vazquez, J. Catal. 189 (2000) 147.